Enhancing hydrogen storage properties of the Mg/MgH2 system by the addition of bis(tricyclohexylphosphine)nickel(II) dichloride

B. Galey, A. Auroux, Sylviane Sabo-Etienne, Mary Grellier, G. Postole

Enhancing hydrogen storage properties of the Mg/MgH_2 system by the addition of bis(tricyclohexylphosphine)nickel(II) dichloride

Basile Galey[a], Aline Auroux[a], Sylviane Sabo-Etienne[b], Mary Grellier[b], Georgeta Postole[a*]

[a] *Univ Lyon, Université Claude Bernard Lyon 1, CNRS, IRCELYON, F-69626, Villeurbanne, France*
[b] *LCC-CNRS, Université de Toulouse, CNRS, UPS, 205 route de Narbonne, BP 44099, F-31077 Toulouse Cedex 4, France.*

Corresponding author: georgeta.postole@ircelyon.univ-lyon1.fr

Abstract

This is a first report on the use of the bis(tricyclohexylphosphine)nickel(II) dichloride complex (abbreviated as NiPCy3) into MgH_2 based hydrogen storage systems. Different composites were prepared by planetary ball-milling by doping MgH_2 with (i) free tricyclohexylphosphine (PCy3) without or with nickel nanoparticles, (ii) different NiPCy3 contents (5 – 20 wt%) and (iii) nickel and iron nanoparticles with/without NiPCy3. The microstructural characterization of these composites before/after dehydrogenation was performed by TGA, XRD, NMR and SEM-EDX. Their hydrogen absorption/desorption kinetics were measured by TPD, DSC and PCT. All MgH_2 composites showed much better dehydrogenation properties than the pure ball-milled MgH_2. The hydrogen absorption/release kinetics of the Mg/MgH_2 system were significantly enhanced by doping with only 5 wt% of NiPCy3 (0.42 wt% Ni); the mixture desorbed H_2 starting at 220 °C and absorbed 6.2 wt% of H_2 in 5 min at 200 °C under 30 bars of hydrogen. This remarkable storage performance was not preserved upon cycling due to the complex decomposition during the dehydrogenation process. The hydrogen storage properties of NiPCy3-MgH_2 were improved and stabilized by the addition of Ni and Fe nanoparticles. The formed system released hydrogen at temperatures below 200 °C, absorbed 4 wt% of H_2 in less than 5 min at 100 °C, and presented good reversible hydriding/dehydriding cycles. A study of the different storage systems leads to the conclusion that the NiPCy3 complex acts by restricting the crystal size growth of Mg/MgH_2, catalyzing the H_2 release, and homogeneously dispersing nickel over the Mg/MgH_2 surface.

Keywords

Hydrogen storage, MgH_2, bis(tricyclohexylphosphine)nickel(II) dichloride complex, absorption, desorption, reversibility.

1. Introduction

Hydrogen has been widely identified as a promising and clean energy carrier for the future, as a way to store energy and also as an attractive substitute to fossil fuels in the transportation area [1–5] Storing hydrogen in a safe and efficient way is a key challenge for the large-scale use of hydrogen in both stationary and mobile applications [6,7]. Nowadays, it is mostly stored under pressure, but, hydrogen being the lightest element, very high pressures are required to reduce the volume, which leads to safety and cost issues [8]. Liquid storage is hardly practicable as cryogenic temperatures are required to maintain hydrogen under this physical form. Hydrogen storage in solid-state materials like metal/metal hydride systems, stable compounds at moderate pressures and temperatures able to reversibly absorb large amounts of hydrogen, is highly desirable for the hydrogen sector development and especially for mobile applications [9].

Magnesium/magnesium hydride system has been under focus as a favorable hydrogen storage medium since the late 1960s [10]. Its advantages, potential applications and limitations have been discussed in different review articles [10–16]. In summary, magnesium is an abundant element, cheap, recyclable, lightweight and non toxic. Theoretically, it can reversibly absorb 7.65 wt% of hydrogen to form magnesium hydride, MgH_2, a stable compound under normal conditions of temperature and pressure. Mg/MgH_2 systems have been extensively investigated as solid-state hydrogen storage material for mobile and stationary applications without [10–12,17] or in combination with a heat storage media (e.g. adiabatic tanks [18]) and as potential electrode materials in solid-state ion batteries [19,20]. However, challenges remain for large-scale implementation. Indeed, the systems based on MgH_2 present significant net energy loss due to its high thermodynamic stability (decomposition enthalpy of 75 kJ/mol H_2 [13,21]) necessitating temperatures exceeding 300 °C at 1 bar H_2 for hydrogen release [14]. Furthermore, the system suffers from slow sorption kinetics limiting the rate at which hydrogen can be stored and released, and poor stability of hydrogen sorption performance during cyclic dehydrogenation/re-hydrogenation at high temperatures [10,15]. Additionally, because MgH_2 has very low thermal conductivity and the absorption/desorption of hydrogen are exothermic and respectively endothermic reactions, heat transport in the material can affect the sorption properties of the system [22]. Consequently, the challenge for the use of Mg/MgH_2 storage systems is to enhance the hydrogenation and dehydrogenation kinetics in order to decrease the storage and delivery temperatures, without losing the high reversible hydrogen storage capacity.

To overcome the drawbacks of the Mg/MgH_2 system, different approaches have been explored in the past decades including (i) surface and structure modification [23–26], (ii) addition of nano-scale transition metals or transition metal oxides as catalytic activators [10,16,27–38] and (iii) formation of composites with other metal hydrides or hydrogen storage materials [39–43]. The impact of these approaches on the hydrogen storage properties of MgH_2 has been the subject of extensive studies [25,27–43] and the main findings have been widely reported in literature reviews [10–16,23,24,26]. Table 1 summarizes part of these reports chosen for the similar experimental conditions (e.g. high-energy milling, thermal analyses performed at a rate of 5 °C/min, apparent activation energy for dehydrogenation determined by DSC analyses) which makes the comparison of results possible.

Table 1 – Literature review of the approaches explored in the past decade to overcome the Mg/MgH_2 system drawbacks – impact on the dehydrogenation properties					
Explored Approach	Experimental conditions	Peak desorption temperature (°C)	Capacity (wt%)	Ea (kJ/mol H_2)	Ref.
None – commercial MgH_2		≈420	7.1	n.d.	[31]
		437	7.0	239	[45]
Nanostructuration by grinding	1 h milling	≈370	7.2≠	167	[31]
	5 h milling	354	7.0≠	162	[36]
	5 h milling	346	6.8≠	176	[45]
Addition of transition metals	≈2.2 wt% Ni nano	≈210	6.5	94*	[27]
	5 wt% Fe nano	≈225	6.3	74	[28]
Addition of metals oxides	10 wt% $TiVO_{3.5}$	≈250	6.8	62.4	[29]
	10 wt% Ni/TiO_2	231	6.5	44	[30]
	≈18 wt% Li_2TiO_3	211	6.0	84	[38]
Formation of composites	Mg_2NiH_4	240	3.5	103	[42]
	Mg-La-Fe-H	250	5.5	100.3	[43]
Addition of complexes	10 wt% $Ni(C_5H_5)_2$	≈300	7.0	110	[44]
	5 wt% $RuH_2(H_2)_2(PCy_3)_2$	331	6.4	141	[45]

n.d. = not determined

≠ The differences observed in the storage capacity are due to the purity of the starting MgH_2.

* Determined for ≈4.4 wt% Ni

The lowest hydrogen desorption temperatures are observed when MgH_2 is doped with transition metal based additives (nanoparticles or oxides), but the resulting systems suffer generally from poor operational cycle lifespans because of sintering and oxidation issues [27]. However, the use of high amounts of catalytic phase allows better behavior upon cycling [29]. Metal hydride composites also allow to overcome the lifespan issue, but the storage capacities of the formed alloys are most of the time low [42,43]. The studies aimed at assessing the potential of Mg/MgH_2 as a hydrogen storage system by doping with transition metal complexes are scarce. Kumar et al. [44] used bis(cyclopentadienyl) nickel II complex (10 wt%) as a precursor for homogeneous doping of nickel (3.1 wt%) over the MgH_2 surface during ball milling. Both hydrogen absorption and desorption temperatures of Mg/MgH_2 system were decreased by doping. However, the authors neither address in this study the reversibility issue after sorption cycling, nor the role of the organic derived species formed during milling, which can enhance the dehydrogenation properties as we have recently shown in [45]. In our previous work, we studied the impact of two bis-dihydrogen ruthenium complexes on the hydrogen storage properties of Mg/MgH_2. We observed that during ball milling with MgH_2, the complexes act as precursors to the ruthenium active species and give rise to an organic coating at the surface of the MgH_2 particles. The hydrogen storage properties of the Mg/MgH_2 + complexes mixtures were significantly enhanced compared to Mg/MgH_2. The improved dehydrogenation properties of MgH_2 were found to be related to the active organic species formed during milling preparation. The presence of ruthenium metallic centers coming from the complexes did not show a significant impact on the MgH_2 decomposition kinetics but considerably improved the Mg hydrogen absorption kinetics. Addressing the reversibility issue, we showed that the poor cycling stability was directly related with the low thermal stability of the complexes which decomposed around 150 °C. By modifying the nature of the ligands and/or the metallic center of such complexes, further reduction of the hydrogen release temperature can be anticipated, thus approaching a range where reversibility could be feasible.

The present study follows previous works [44,45] related to the use of transition metal complexes and shows the impact of the thermal stability of the complex and of the nature of the transition metal center on the storage properties of the Mg/MgH_2 system. The addition of bis(tricyclohexylphosphine)nickel(II) dichloride complex, $(NiCl_2(PCy_3)_2$ labeled NiPCy3 throughout the paper) as doping agent to MgH_2 is reported on for the first time. This family of complex is often used as catalyst in water oxidizing and cross-coupling reactions [46–49]. NiPCy3 complex decomposes at 284 °C and is formed with a nickel center, a transition metal known for enhancing both formation and decomposition kinetics of MgH_2 [27,30,36,42,44]. The hydrogenation properties of the "MgH_2 + bis(tricyclohexylphosphine)nickel(II) dichloride complex" mixture prepared by ball milling are investigated via volumetric measurements. The effect of the milling process on the microstructural properties of the obtained storage system is studied by X-ray diffraction (XRD), scanning electron microscopy (SEM-EDX) and nuclear magnetic resonance spectroscopy (solid-state NMR). The kinetic properties of MgH_2 decomposition are determined by Temperature Programmed Desorption (TPD) and calorimetric (DSC) measurements. For comparison, the effect on the storage properties of doping magnesium hydride with free tricyclohexylphosphines (PCy3) and metallic (Ni, Fe) nanoparticles is also investigated.

2. Experimental

2.1. Materials

The magnesium hydride powder was provided by McPhy Company (La Motte-Fanjas, France) and its physico-chemical and hydrogen storage properties are reported elsewhere [45]. XRD patterns revealed the presence of low amounts of Mg and MgO (5 and 4 wt%, respectively, as evaluated from Rietveld refinement) in as-received MgH_2 and a mean size of crystallites of about 200 nm. The hydrogen storage capacity of the Mg/MgH_2 system was measured to be 7 wt%, as expected given the powder purity. The MgH_2 decomposes at temperatures higher than 400 °C.

The organic additives (bis- (tricyclohexylphosphine)nickel(II) dichloride complex of 97% purity and free tricyclohexylphosphine of >94% purity) and the metallic nanoparticles (Ni and Fe/C of average particle sizes <100 nm and 25 nm respectively) used in this study were purchased from Sigma-Aldrich. Fig. 1 shows the schematic representation of the organic species namely here NiPCy3 for the nickel complex $NiCl_2(PCy_3)_2$, and PCy3 for free tricyclohexylphosphine.

bis(tricyclohexylphosphine)nickel(II) dichloride complex
$C_{36}H_{66}Cl_2NiP_2$
"NiPCy3"

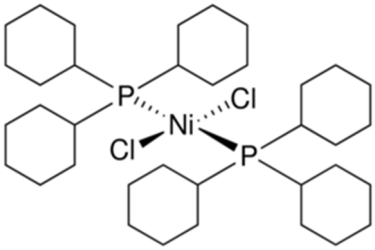

tricyclohexylphosphines
$(C_6H_{11})_3P$
"PCy3"

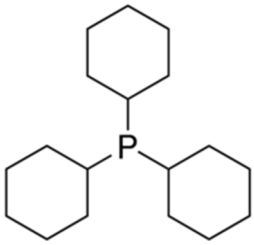

Fig. 1 – Schematic representation of the organic additives used in the study.

All the mixtures of MgH_2 with different additives (organic species and metallic nanoparticles) were prepared by planetary ball milling using a PM100 apparatus from Retsch under an inert argon atmosphere. The milling bowl was hermetically closed inside the glovebox to prevent any oxidation of the powders. The MgH_2 based storage systems were obtained by milling for 5 h using balls of zirconium dioxide of 1 mm diameter and a milling frequency of 300 revolutions per minute. The ball to powder mass ratio was 100:1. The rotation of the ball in the mill was paused every 2 min and inverted every 5 min to limit the temperature increase in the milling cell. For comparison, MgH_2 was milled under the same conditions without any additive and the obtained powder is denoted as m-MgH_2. Table 2 shows the different MgH_2-based mixtures studied in this work and the labels used further on for these storage systems.

Table 2: Studied MgH_2-based storage systems: label and composition

System label	Metallic nanoparticles (wt%)		Organic additives (wt%)		MgH_2 (wt%)
	Ni	Fe/C	NiPCy3	PCy3	
5-PCy3	-	-	-	5	95
5-NiPCy3	-	-	5	-	95
20-NiPCy3	-	-	20	-	80
20-(Ni+PCy3)	1.7	-	-	16.2	82.1
NiFe-NiPCy3	10	5	5	-	80
NiFe	10	5	-	-	85

Two composites have been prepared by milling MgH_2 with respectively 5 and 20 wt% of NiPCy3 complex (5-NiPCy3 and 20-NiPCy3, labeled in relation to the complex used as additive and its amount, Table 2). For a better understanding of how the complex can impact the absorption and desorption kinetics of the Mg/MgH_2 system, MgH_2 was also doped with free tricyclohexylphosphines (PCy3) and nickel nanoparticles (Ni_{nano}). In order to achieve Ni and PCy3 contents similar to 20 wt% of Ni-complex, 1.7 wt% of Ni_{nano} and 16.2 wt% of PCy3 were added to MgH_2 before milling and the system obtained was labelled 20-(Ni+PCy3). The effect of free tricyclohexylphosphines on the storage properties of Mg/MgH_2 was also investigated by the preparing of a mixture "MgH_2 + 5 wt% of PCy3" (5-PCy3). Finally, based on literature reports claiming the benefic effects of nickel and iron on the storage properties of Mg/MgH_2, systems containing Ni and Fe nanoparticles were also prepared. For this, MgH_2 was co-milled with both Ni (10 wt%) and Fe (5 wt%) in the absence and in the presence of 5 wt% of NiPCy3 complex. The obtained mixtures were labelled NiFe (without NiPCy3 complex) and NiFe-NiPCy3 (with NiPCy3 complex).

2.2. Characterization

The temperature stability of the additives was analyzed by Thermogravimetric Analysis (TGA) with a TG Discovery from TA Instruments. The analyses were performed from ambient to 450 °C (heating rate of 2 °C/min) under an argon flow of 25 mL/min. Hermetic aluminum pans with a pin hole, sealed inside the glove box, were used to prevent any oxidation.

The XRD structural characterization of the samples was carried out with a Bruker D8 Advance A25-ray diffractometer using Cu–Kα radiation. The diffraction patterns were analyzed by the Rietveld

method, using the Topas software to determine the phase composition and crystallites mean size. X-ray sample holders were filled inside the glove box and covered with a kapton foil to minimize air contact during X-ray measurements.

The sample morphology was characterized by Scanning Electron Microscopy (SEM) with a Philips 5800 apparatus. The powders were dispersed on carbon grids using ethanol. The mean size and size distribution of the MgH_2 particles were determined from SEM images, using ImageJ software to count the particles. Energy-dispersive X-ray (EDX) analyses were carried out in parallel with SEM measurements in order to determine the presence of different elements in the samples (e.g. Ni, Fe, O, Mg...).

^{31}P solid-state NMR experiments were performed on a Bruker Advance III 500WB spectrometer equipped with a 4 mm probe at 202.4 MHz. The chemical shifts of ^{31}P nuclei are given relative to H_3PO_4 at 0 ppm.

2.3. Storage properties

The hydrogen desorption properties of the different storage systems were studied by Temperature Programmed Desorption (TPD) with a TPD/R/O-1100 apparatus from Thermo. The analyses were performed from ambient temperature to 450 °C (2 °C/min) under an argon flow of 20 mL/min. A calibration curve obtained from the reduction of different masses of copper (II) oxide was used to determine the amount of hydrogen desorbed by the samples.

Calorimetric measurements were performed with a DSC Q100 from TA Instruments by using hermetic aluminum pans with a pin hole, sealed inside the glovebox. The measurements were carried out under a flow of high-purity argon (40 mL/min) at different heating rates (2, 5, 7.5 and 10 °C/min) from room temperature to 450 °C. The apparent activation energy of the samples was determined using Kissinger's method as described in the ESI (eqn. S1) [50,51].

The absorption kinetics were measured by a volumetric method with a HVPA-200 Sievert apparatus from Micromeritics. The absorptions were performed at 100, 200 and 300 °C under 30 bar of H_2 and the absorption rates were calculated at 80 % of the maximum capacity of the sample. Before the isotherms, the powders were outgassed under vacuum at temperatures between 200 and 300 °C (the lowest temperature possible based on the TPD data to ensure the complete desorption of hydrogen).

Finally, in order to study the reversibility of the formed storage systems, hydrogen absorption/desorption cycles were performed under three different temperature conditions:

- "Hard" conditions: desorption under vacuum at 300 °C and absorption under 30 bars of H_2 at 300 °C,
- "Medium" conditions: desorption under vacuum at 225 °C and absorption under 30 bars of H_2 at 200 °C,
- "Mild" conditions: desorption under vacuum at 200 °C and absorption under 30 bars of H_2 at 100 °C.

The evolution of the hydrogen release properties of the different storage systems was monitored by performing TPD analyses from ambient temperature to 450 °C (2 °C/min) under argon flow (20

mL/min) after each dehydrogenation/hydrogenation cycle. The results obtained were compared with the hydrogen desorption properties of the powders immediately after milling.

3. Results and discussion

3.1. Thermal stability of the organic additives: TGA analyses

Fig. 2 presents the thermogravimetric analyses for the two additives used in this study, the free phosphine PCy3 and the nickel complex NiPCy3. Mass loss and DTG signals are presented as a function of temperature. The decomposition of free tricyclohexylphosphine starts around 100 °C, reaches its maximum rate at 231 °C, and is complete at 250 °C. The Ni-based complex shows a higher thermal stability compared to PCy3. The beginning of its decomposition is observed at around 270 °C with the maximum weight loss rate at 280 °C. At 450 °C, the complex is decomposed at 81.6 wt%, the remaining 18.4 wt% corresponding to the mass of the Ni and Cl atoms present in NiPCy3 (theoretical value of 18.5 wt%). Therefore only the tricyclohexylphosphine ligands of NiPCy3 decompose in this temperature range.

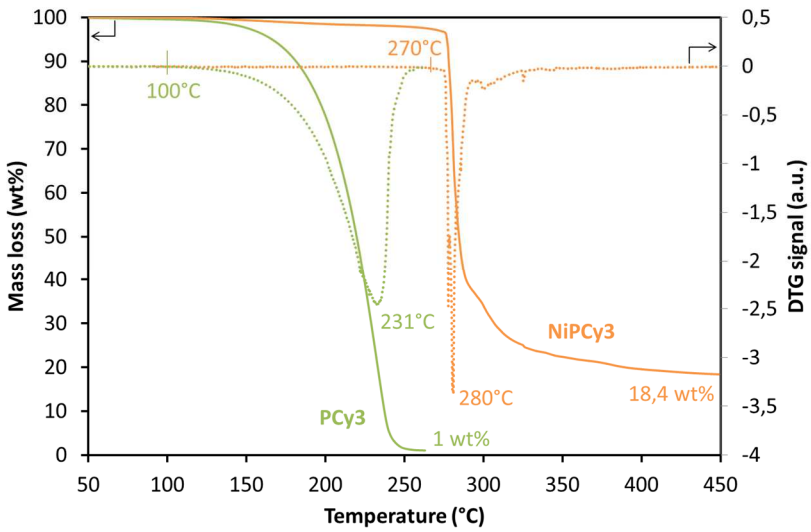

Fig. 2 – Thermogravimetric analyses: mass loss and DTG signal of the organic additives heated under argon to 450 °C at 2 °C/min.

3.2. Microstructural characterization of the mixtures: XRD, SEM and NMR analyses

Although reported elsewhere [45], the physico-chemical and storage properties of milled MgH_2 (m-MgH_2) are also given for the sake of comparison with the new systems studied here.

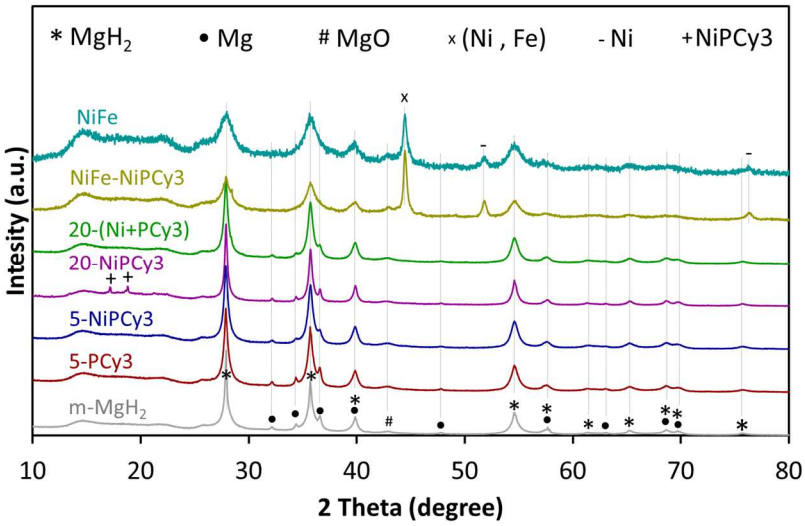

Fig. 3 – X-ray diffraction patterns of the studied samples.

Fig. 3 presents the as-prepared powder XRD patterns. The samples are mostly composed of magnesium hydride with traces of metallic magnesium and magnesium oxide, as also detected in as-received MgH_2 [45]. For all samples, the amount of nickel in the mixtures is expected to be close to the theoretical one, taking into account the ball milling method of preparation and the thermal stability of the additives. The absence of characteristic nickel diffraction peaks in the samples doped with NiPCy3 and (Ni+PCy3) could be due to the low amounts involved (0.4, 1.7 and 1.7 wt% for 5-NiPCy3, 20-NiPCy3 and 20-(Ni+PCy3), respectively) and to its homogeneous dispersion on the MgH_2 surface. For 20-NiPCy3, peaks corresponding to carbon-based species are noticed at 17.2 and 18.8°, which were not further analyzed due to their appearance in the Kapton foil *2 Theta* region (used to protect the sample from oxidation). Characteristic diffraction lines of Ni and Fe are detected for NiFe-NiPCy3 and NiFe systems containing much higher amounts of nickel (10 wt%) and iron (5 wt%) when compared with only complex-based powders.

Table 3 – Average crystal sizes of the prepared samples

Samples	Crystal size (nm)
NiFe	10 ± 3
NiFe-NiPCy3	12 ± 4
20-(Ni+PCy3)	17 ± 3
20-NiPCy3	23 ± 5
5-NiPCy3	17 ± 2
5-PCy3	17 ± 3
m-MgH_2	34 ± 13

Table 3 presents the mean sizes of MgH_2 crystallites for the prepared samples, as determined by the Rietveld method. Milling as received MgH_2 significantly reduces its mean crystallite size from ≈213 to ≈34 nm [45]. The grinding is even more effective in the presence of the organic additives with mean crystallite size decreasing to around 17 nm. The use of free tricyclohexylphosphine or Ni-based complex may reduce the cold welding of the MgH_2 particles during milling preventing further aggregation. For NiFe-NiPCy3 and NiFe, further crystal size reduction is observed, probably because of ductility differences between the metallic nanoparticles and MgH_2 [52].

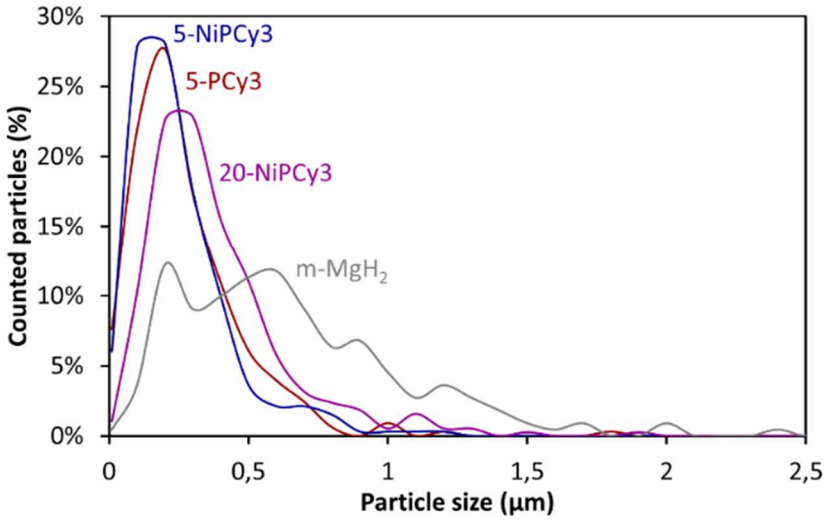

Fig. 4 – MgH_2 particles size distribution within the samples, measured by SEM analyses.

The MgH_2 particle size distributions within m-MgH_2, 5-PCy3, 5-NiPCy3 and 20-NiPCy3 samples were obtained from SEM micrographs as presented in Fig. 4. It is observed that the particle size distribution is broader in m-MgH_2 than in the other samples. No major differences can be noticed between 5-PCy3, 5-NiPCy3 and 20-NiPCy3, except a shift toward slightly larger particles for 20-NiPCy3 as also observed by XRD (Table 3). This difference may be explained by the use of 20 wt% of complex in 20-NiPCy3 mixture. Indeed, NiPCy3 is a softer material than MgH_2 and its presence in high amount may reduce the milling efficiency. The MgH_2 particle size distributions confirm the limitation of the powder aggregation in presence of the organic additives.

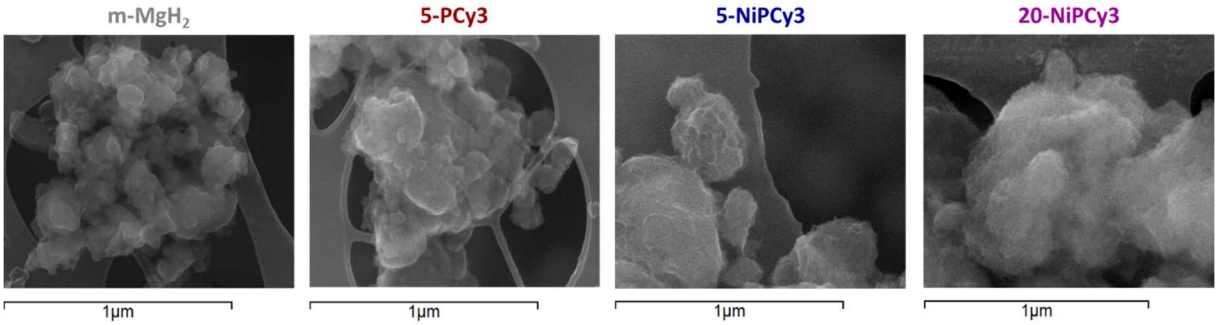

Fig. 5 – SEM images of the prepared samples.

The morphology of the samples was also studied by SEM imaging. Fig. 5 shows the obtained micrographs for m-MgH_2, 5-PCy3, 5-NiPCy3 and 20-NiPCy3. EDX analyses and corresponding SEM images for NiFe-NiPCy3, 20-NiPCy3 and NiFe systems are given in Fig. S1. For the samples doped with NiPCy3 complex, an organic coating shell surrounding MgH_2 particles is observed, modifying their morphology (Fig. 5). Such coating is not visible in 5-PCy3 which can be explained by a possible partial decomposition of PCy3 during milling. The presence of a homogeneously dispersed organic phase in

the systems containing NiPCy3 can be related to its higher stability compared to PCy3. No information can be given concerning this organic phase structure. The EDX analyses of these mixtures (see for example 20-NiPCy3 in Fig. S1) indicate the presence of phosphorus, chlorine and nickel together with magnesium. Oxygen is also detected due to both the EDX experimental conditions and the presence of some MgO in the starting MgH_2 powder, as observed by XRD. As expected, the amount of nickel determined by EDX is close to that in the additives (e.g. 1.5 wt% Ni in 20-NiPCy3 while 1.7 wt% Ni are present in 20 wt% of NiPCy3 complex). It is worth noticing that iron is also detected by EDX for NiFe-NiPCy3 and NiFe systems.

To further investigate if the structure of the NiPCy3 complex was preserved during ball-milling with MgH_2, ^{31}P solid-state NMR experiments were performed. In Fig. 6 the main spectroscopic features of the starting complex NiPCy3 and of free PCy3 are compared with those of 5-PCy3, 5-NiPCy3, 20-NiPCy3 and 20-(Ni+PCy3) samples. Free PCy3 displays a ^{31}P NMR signal at 6.8 ppm shifted at 9.8 ppm in 5-PCy3. This result means that by milling free tricyclohexylphosphine with MgH_2 a new phosphorus based species is in situ formed. Interestingly, 5-NiPCy3 presents a similar signal at 9.8 ppm. This signal is significantly shifted from that of the starting complex NiPCy3 which resonates at 1.9 ppm. Further, as seen in Fig. 6 for 20-NiPCy3, by increasing the amount of complex, the signal at 9.8 ppm is accompanied by a second signal at 6.8 ppm which corresponds to the signal of free PCy3. This indicates that in spite of the higher thermal stability of NiPCy3 in comparison with PCy3, the degradation of the complex takes place during milling, and the released PCy3 partly interacts with MgH_2 to form new phosphine based species. The presence of the signal corresponding to free phosphines with increasing amount of complex and/or PCy3 may be the result of a complete coverage of the MgH_2 surface by the new formed species. Indeed, 20-(Ni+PCy3) presents similar signals to those observed for 20-NiPCy3 as two main signals are detected by ^{31}P NMR at 9.8 and 6.8 ppm together with a minor one at 8.4 ppm. This suggests that nickel nanoparticles partly interact with free tricyclohexylphosphine to form Ni/phosphine derived species dispersed on the MgH_2 surface during milling.

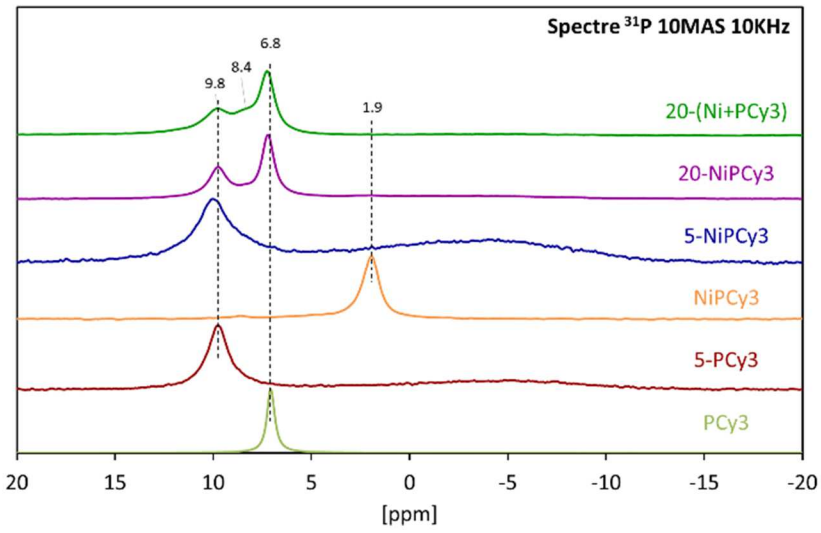

Fig. 6 – ^{31}P NMR spectra of the studied systems. Comparison with PCy3 and NiPCy3.

3.3. Hydrogen desorption properties: TPD and DSC analysis

The impact of the additives on MgH_2 decomposition was studied by TPD analysis. Fig. 7a displays the TPD plots while the evolution of the amount of hydrogen desorbed as a function of temperature is given in Fig. 7b. In Table 4, the onset and desorption peak maximum temperatures as well as the amount of hydrogen released are summarized together with the apparent activation energy of MgH_2 decomposition. To calculate the apparent activation energy, DSC analyses were performed at different heating rates (Fig. S2) and the values were determined using Kissinger's method (Fig. S3).

As shown on Fig. 7, m-MgH_2 desorbs 6.8 wt% of hydrogen within a broad temperature range (300 to 400 °C). The amount of hydrogen evolved is slightly lower than for as-received MgH_2 [45], probably due to partial MgH_2 decomposition during ball-milling. The MgH_2 crystal size reduction during milling induced both a decrease of the hydrogen desorption temperature (by 81 °C) and of the apparent activation energy (by 36 %) compared to as-received powder. The broad hydrogen desorption TPD profile presenting two maxima at 330 and 360 °C as observed in Fig. 7a are due to the large particle size distribution in m-MgH_2 (peaks at 200, 600, 900 and 1200 nm, Fig. 4).

The doped systems exhibit improved hydrogen desorption properties compared to pure milled MgH_2 powder. The onset temperatures of hydrogen desorption are up to 100 °C lower than that of m-MgH_2, most probably due to the synergetic effects of crystal size reduction and formation of catalytic active sites derived from the organic additives during milling. Generally, the TPD peaks are narrower and show only one desorption peak (Fig. 7a), consistent with the monomodal MgH_2 particle size distribution within these samples (centered on 200 nm, Fig. 4). The amount of released hydrogen varies between 6.5 and 5.3 wt% depending on the quantity of added dopant.

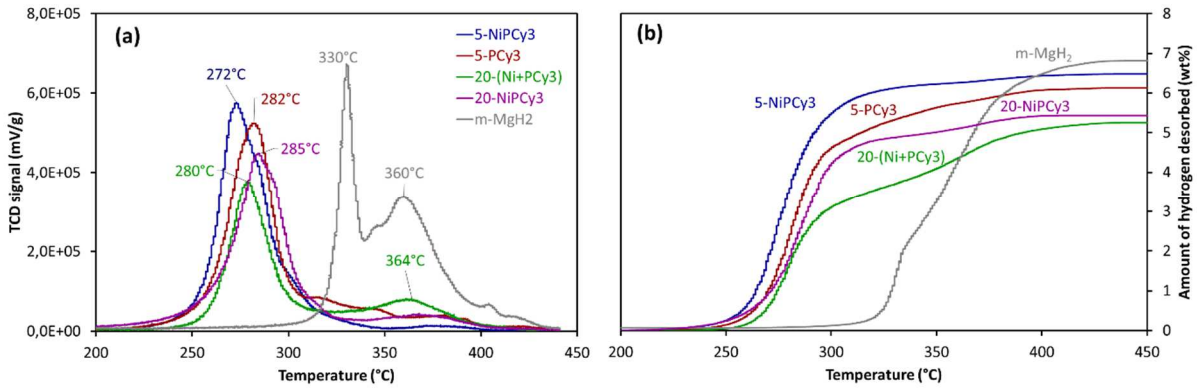

Fig. 7 – (a) TPD profiles and (b) corresponding thermally programmed H_2 desorption capacities curves of studied MgH_2-based powders. Experiments performed under argon from 40 to 450 °C with a heating rate of 2 °C/min.

Table 4 – Hydrogen desorption properties of the samples obtained by TPD and DSC					
Samples	TPD				DSC
	Onset temperature (°C)	Peak temperature (°C)	Hydrogen released [a] (wt%)	Normalized hydrogen released [b] (wt%)	Activation energy (kJ/mol)
m-MgH_2	310	330 – 360	6.8	7.5	176
5-PCy3	232	282	6.1	7.1	126
5-NiPCy3	221	272	6.5	7.5	145
20-NiPCy3	208	285	5.4	7.7	196
20-(Ni+PCy3)	243	280 – 364	5.3	7.4	n.d.[c]

[a] g_{H_2}/g_{sample}
[b] g_{H_2}/g_{MgH_2}
[c] Not determined.

5-NiPCy3 composite shows the best hydrogen release properties among all the presented systems, with the maximum of desorption at 272 °C and almost the same amount of H_2 desorbed as in m-MgH_2. A low quantity of complex containing only about 0.4 wt% of nickel is thus able to significantly improve the storage properties of MgH_2 without reducing its high hydrogen capacity. Interestingly, the TPD experiments indicate that PCy3 also reduces the decomposition temperature of MgH_2. The thermodesorption curve of 5-PCy3, slightly shifted towards higher temperatures compared to 5-NiPCy3, presents a maximum of hydrogen release at 282 °C and small peaks in between 300 and 400 °C. No nickel is involved in this sample, and the better hydrogen storage properties of 5-PCy3 compared to m-MgH_2 cannot be only explained by the MgH_2 particle size difference (i.e. presence of particles around 200 nm in both samples as seen in Fig. 4, but different hydrogen release temperatures, Fig. 7a). Therefore the significant kinetic impact observed at temperatures below 300 °C must be related with the phosphorus-based species formed by the partial decomposition of PCy3 during milling as revealed by NMR. The enhancement of the dehydrogenation properties of nanoconfined MgH_2 by P-doping has already been reported [53] based on both theoretical and experimental investigations. He et al. [53] demonstrated by using density functional theory calculations that the reaction energy for the release of one H_2 can be reduced in the presence of phosphorus to 0.20 eV, versus 0.75 eV for bulk MgH_2.

The shift toward lower MgH_2 decomposition temperatures for 5-NiPCy3 in comparison with 5-PCy3 may be explained by the presence of nickel and its important kinetic impact on H_2 desorption as widely reported in the literature [30,42,44]. Although the synergetic catalytic effect of Ni and in-situ formed phosphorus based active species is evident (decrease in the dehydrogenation peak temperature and increase of the dehydrogenation capacity in the presence of Ni) the nickel content is too low for a more pronounced kinetic impact.

Increasing the amount of nickel in the storage system should enhance the MgH_2 dehydrogenation kinetics [27,35,36]. MgH_2 milled with 20 wt% of NiPCy3 was therefore studied and the thermodesorption curve is also given in Fig. 7. It can be seen that 20-NiPCy3 releases hydrogen at higher temperatures than 5-NiPCy3, despite a content of nickel 4 times higher (Table 4). This surprising behavior can be explained by the presence of chlorine in NiPCy3 complex reported as kinetics inhibitor for MgH_2 decomposition [31,32,54]. The expected impact of Ni on kinetics in sample 20-NiPCy3 seems therefore to be overcome by the negative impact of chlorine and its increased amount.

The hydrogen release properties of 20-(Ni+PCy3) composite were further investigated. As shown in the experimental part, this system, free of chlorine, contains similar amounts of Ni (1.7 wt% added as nanoparticles) and PCy3 (16.2 wt%) as in 20 wt% of NiPCy3. 20-(Ni+PCy3) composite desorbs 5.3 wt% of H_2, similar to 20-NiPCy3, but in a two-step process. The main hydrogen desorption takes place at 280 °C, followed by a small desorption peak at 364 °C (Fig. 7a). Surprisingly, the principal TPD peak is shifted towards higher temperatures compared to 5-NiPCy3 despite a higher content of nickel and no chlorine present. This may be caused by the larger size of the nickel nanoparticles and possibly their non-uniform distribution on MgH_2 surface when added in the presence of PCy3. Comparing these results with those obtained when doping MgH_2 with 5 wt% of NiPCy3 complex (only 0.4 wt% of Ni) it can be concluded that a small amount of catalyst is sufficient to improve the reaction kinetics when very small metal catalyst particles are uniformly distributed on the MgH_2 surface (it is worth mentioning that in NiPCy3, each complex molecule contains only one nickel atom.) This agrees with former research suggesting that the Ni particle size would influence its catalytic effect on the MgH_2 decomposition [27,30].

The activation energies for hydrogen desorption of the different composites were determined and shown in Table 4. The apparent activation energy value for 5-PCy3 composite is 126 kJ/mol. This value is much lower than that of pure-milled MgH_2 (176 kJ/mol) in agreement with the observed decrease of hydrogen release temperature upon doping with PCy3. The apparent activation energy of 5-NiPCy3 decomposition is higher than in 5-PCy3 (145 kJ/mol vs. 126 kJ/mol). This result is unexpected as the temperature of hydrogen desorption is lower in 5-NiPCy3 than in 5-PCy3. The apparent activation energy of 20-NiPCy3 is even higher (196 kJ/mol). It is likely that the values obtained for the apparent activation energies do not correspond to MgH_2 decomposition only, being in disagreement with the improved hydrogen desorption kinetics observed by TPD. To further verify this hypothesis, DSC experiments at different heating rates were performed for NiPCy3 complex (Fig. S4). An endothermic peak is present around 280-300 °C with an apparent activation energy of 368 kJ/mol. With a temperature range close to that of MgH_2 decomposition in 5-NiPCy3 and 20-NiPCy3 samples, the contribution of NiPCy3 to the apparent activation energy of the mixtures is therefore significant and can explain the high values observed.

3.4. Reversibility of the systems: PCT and TPD analysis

Achieving reversibility of hydrogen absorption/desorption is a major step in the conception of an efficient hydrogen storage system. This point is addressed here for 5-NiPCy3 composite, which shows the best hydrogen released properties between the different tested systems so far.

The hydrogen absorption properties were investigated at 200 °C under 30 bars of hydrogen by using a Sievert's apparatus. After each absorption step, the evolution of the hydrogen release properties was followed by TPD. The results obtained are presented in Fig. 8. The nickel complex shows a significant positive impact on the hydrogen absorption kinetics, 5-NiPCy3 composite adsorbing 6.1 wt% of hydrogen within 5 min (rate of 0.07 wt%/s). This rate is substantially faster than observed for dehydrogenated m-MgH_2 (6.0 wt% H_2 in 225 min, 0.0006 wt%/s, as reported earlier [45]).

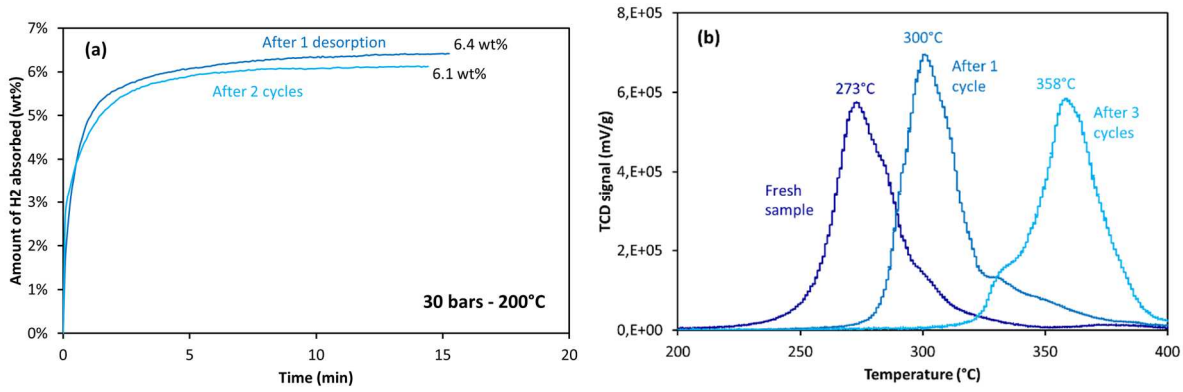

Fig. 8 – (a) the isothermal rates of hydrogen absorption and (b) TPD profiles, for 5-NiPCy3 composite. Comparison between just after milling and after cycling under the "medium" temperature conditions (absorption 200 °C, desorption 225°C)

As observed in Fig. 8a, the absorption curve recorded after two dehydrogenation/hydrogenation cycles is very similar to the initial one, and the hydrogen absorption rate only slightly decreases (5.9 wt% H_2 within 5 min, 0.06 wt%/s). The slight decrease in the capacity during cycling may be the result of particle growth of both MgH_2 and Ni. Taking into account that the decomposition of the complex organic part is expected during the first dehydrogenation step with loss of the phosphorus based species [45], only the kinetic effect of dispersed nickel is observed during hydrogenation steps.

The evolution of the hydrogen desorption rates is presented in Fig. 8b where the TPD curve obtained for the fresh 5-NiPCy3 composite is compared with those after 1 and 3 absorption/desorption cycles. A strong change in the hydrogen desorption behavior is observed after only one sorption cycle, and the sharp decrease in the kinetics of MgH_2 decomposition accentuates with the following cycles. The same general trend of slower dehydrogenation kinetics with cycling was observed in [45] and for m-MgH_2 and 5-PCy3 systems (Fig. S5). This phenomenon can be attributed to the growth of MgH_2 crystallites during cycling as confirmed by XRD analyses (Table S1, Fig. S6). The decomposition of the complex organic part during dehydrogenation step, and hence the loss of the protective coating around MgH_2 particles, may accelerate the sintering process of 5-NiPCy3. Furthermore, the positive impact of the active phosphorus based species [53] on the release of hydrogen is also lost by their decomposition and desorption under vacuum in the experimental conditions used (no ^{31}P signal visible after cycling, [45]). The low amount of nickel in the composite, although enough for preserving the absorption properties during cycling (Fig. 8a), is too low to maintain the desorption kinetics at high level. An increase in the amount of metallic active sites is expected to reduce the temperature of H_2 release in MgH_2 enough to limit the decomposition of the organic part of the complex.

3.5. Optimization for a reversible storage system: NiFe-NiPCy3 composite

The hydrogen storage kinetics of nanostructured MgH_2 doped with different amounts of Ni nanoparticles was investigated by Xie et al. [37]. The authors reported interesting hydrogen storage properties for the 10 wt% Ni doped MgH_2 system, with 6.1 wt% hydrogen desorbed in 10 min at 250 °C under an initial pressure of 0.01 bar of H_2. The enhanced desorption kinetics were mainly attributed to the accelerated combination process of hydrogen atoms by the Ni nanoparticles on the surface of

MgH_2 [37]. When a similar storage system was tested for this study, temperatures higher than 200 °C were needed for complete dehydrogenation under vacuum. Such temperatures are too high for preserving the benefits of NiPCy3 complex which is the aim of this work. Kumar et al. [28] reported that the decomposition of MgH_2 started to occur below 150 °C, with maximum hydrogen desorption at 210 °C, upon the addition of only 5 wt% of iron nanoparticles (nFe). As seen in Fig. S7, such a remarkable behavior was not obtained during our test: MgH_2 catalyzed by 5 wt% of Fe started to decompose at 210 °C, with maximum dehydrogenation at 270 °C. The different behavior may come from the different materials and experimental conditions used. However, these results suggest that both Ni and Fe nanoparticles are effective dopants for catalyzing the dehydrogenation of MgH_2, and by their combination a sufficient synergetic effect is expected on the sorption properties of Mg-MgH_2 system. With this in mind, NiFe-NiPCy3 and NiFe composites were prepared by the addition of nickel (10 wt%) and iron (5 wt%) nanoparticles to MgH_2 with/without 5 wt% of NiPCy3, respectively.

Fig. 9 presents the TPD profiles and corresponding amounts of H_2 desorbed for the two samples just after milling. Clearly, the lowest onset and peak temperatures are obtained for NiFe-NiPCy3 which starts to desorb hydrogen at 175 °C with the TPD peak at 245 °C. This may be explained by the presence of phosphorus-based species in NiFe-NiPCy3 which are not present in NiFe composite. Their kinetic impact on MgH_2 decomposition seems therefore to be combined with that of the Ni and Fe nanoparticles. However, the addition of the complex decreases the overall hydrogen storage capacity to 5.3 wt% in comparison with 5.8 wt% for the NiFe sample.

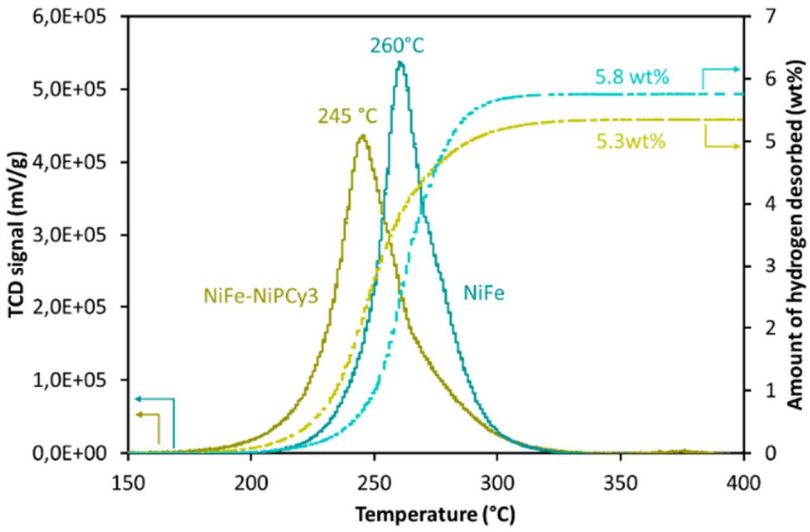

Fig. 9 – TPD profiles and corresponding thermally programmed H_2 desorption curves of NiFe-NiPCy3 and NiFe.

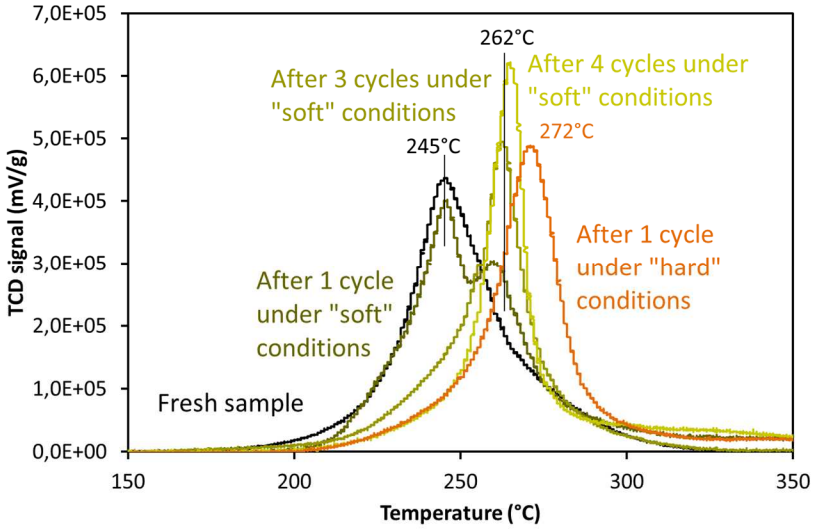

Fig. 10 – TPD profiles of NiFe-NiPCy3 under different cycling conditions. "Soft" conditions: absorption at 100 °C under 30 bars of H_2 and desorption under vacuum at 200 °C. "Hard" conditions: absorption at 300°C under 30 bars of H_2 and desorption under vacuum at 300°C.

Based on the TPD results, the reversibility of the NiFe-NiPCy3 system was studied under the "soft" temperature conditions: absorption under 30 bars of hydrogen at 100 °C and desorption under vacuum at 200 °C. One cycle under the "hard" temperature conditions was also performed for comparison. Fig. 10 compares the TPD profile of the fresh composite with those obtained after 1, 3 and 4 sorption cycles performed under "soft" conditions and 1 cycle performed under "hard" conditions. Fig. 11 presents the corresponding MgH_2 particles size distribution under different cycling conditions and the SEM image of NiFe-NiPCy3 after 1 "soft" cycle. As expected, the dehydrogenation properties of the composite are significantly degraded after only one cycle performed under the "hard" temperature conditions. The decomposition peak shifts towards higher temperatures by almost 30 °C and the sintering of MgH_2 particles is noticeable (Fig. 11). It is worth mentioning that the NiPCy3 complex is completely decomposed under these conditions and the kinetic effect of the phosphorus-based species is lost due to their desorption during the dehydrogenation process.

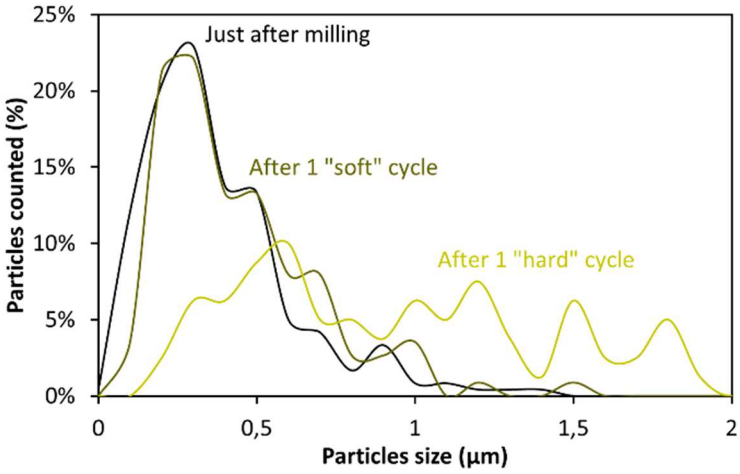

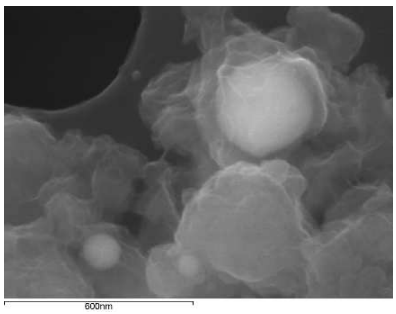

Fig. 11 – MgH_2 particles size distribution within NiFe-NiPCy3 sample under different cycling conditions and corresponding SEM image of NiFe-NiPCy3 after 1 "soft" cycle.

Promising results are obtained when cycling is performed under the "soft" temperature conditions. The decomposition profile splits into two maxima after 1 sorption cycle, with a main peak at 245 °C, similarly to that observed for NiFe-NiPCy3 just after milling. This agrees with SEM data (Fig. 11) showing no MgH_2 particles sintering after the first sorption cycle. The complex is therefore not fully decomposed during the first cycle as also confirmed by SEM analysis (micrograph in Fig. 11), where the organic coating is still visible. The presence of NiPCy3 may restrict the crystal size growth of Mg/MgH_2 and thus further preserve the improved dehydrogenation kinetics during cycling. However, the TPD profile of NiFe-NiPCy3 after 1 cycle shows a minor secondary peak at 262 °C. The presence of this second small peak at higher temperature suggests that (i) besides preventing the sintering of MgH_2 particles, the organic part of the complex has another effect on the dehydrogenation process which is partially lost during cycling and/or (ii) there is a lack of homogeneity in the composite after cycling. Stable hydrogen desorption properties of NiFe-NiPCy3 are obtained after three sorption cycles as it can be seen in Fig. 10, with the maximum rate of dehydrogenation at around 265 °C. Comparing with m-MgH_2, the hydrogen desorption kinetics are significantly improved and these are the best performances obtained for hydrogen release among all the studied composites.

Fig. 12 presents the hydrogen isothermal absorption rate at 100 °C (30 bars of H_2) for NiFe-NiPCy3, NiFe, 5-NiPCy3, 20-NiPCy3 and m-MgH_2. The pure-milled MgH_2 sample shows poor absorption kinetics at 100 °C and less than 0.1 wt% of H_2 is absorbed after 1 hour (absorption rate of 0.00001 wt%/s). Several days would therefore be necessary for complete hydrogen storage. When the nickel complex is added to MgH_2, the H_2 absorption rates increase. A stronger kinetics effect is observed for 5-NiPCy3 when comparing with 20-NiPCy3. At 100 °C, 5-NiPCy3 absorbs 5.8 wt% of H_2 in 1 hour (0.003 wt%/s), versus only 1 wt% for 20-NiPCy3 (0.0003 wt%/s). As for desorption, the addition of a larger amount of complex does not increase the absorption kinetics while the opposite is most of the time reported with increasing amount of catalysts [29,40]. This result is confirming the negative impact of chlorine on the hydrogen storage properties of MgH_2, as also reported in [31,32,54] and observed in *section 3.3*. A remarkable absorption rate at 100 °C, 0.007 wt%/s, is obtained for NiFe-NiPCy3 presenting the best hydrogen absorption properties among all the studied systems. The composite is able to store 4 wt%

of hydrogen in less than 10 min and 5 wt% H_2 in less than 40 min at 100 °C. Interestingly, the absorption rate of NiFe, 0.003 wt%/s, is not as high as that of NiFe-NiPCy3 but rather of the same order as that of 5-NiPCy3.

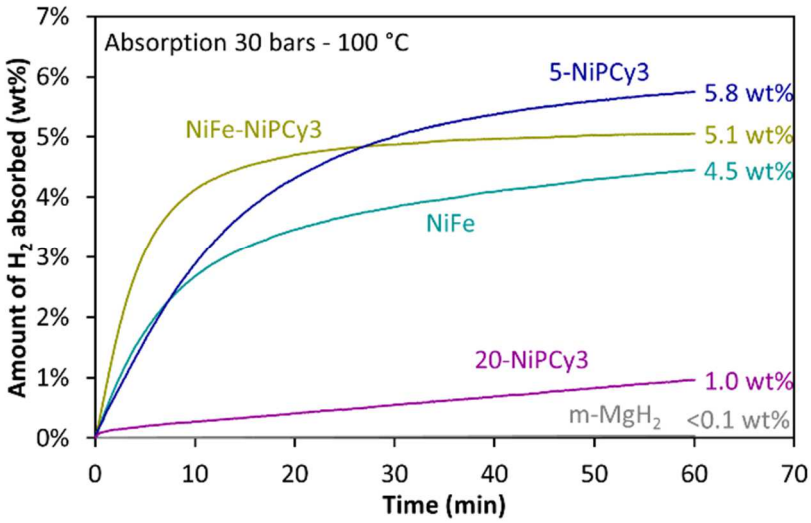

Fig. 12 – The isothermal rates of hydrogen absorption at 100 °C and under 30 bars of H_2.

Xie et al. [55] proposed the formation of a Mg_2Ni phase during dehydrogenation as an explanation for the degradation of hydrogen storage properties of MgH_2 during sorption cycling. The addition of the NiPCy3 complex in the NiFe-NiPCy3 composite may reduce the direct contact of Ni and MgH_2, which should be an effective method to obtain a performant storage system with improved cycling stability.

4. Conclusions

The impact of the bis(tricyclohexylphosphine)nickel(II) dichloride complex (NiPCy3) on the hydrogen storage properties of the Mg/MgH_2 system has been investigated. The role of NiPCy3 was evidenced by studying the effect of free tricyclohexylphosphine (PCy3) without/with nickel particles as well as that of Ni and Fe nanoparticles without/with nickel complex on MgH_2 decomposition.

It was observed that the NiPCy3 complex is combining four significant impacts on the dehydrogenation kinetics of MgH_2:

- The complex forms a coating shell around the MgH_2 particles, reducing the aggregation of the powder during and after milling.
- The in situ phosphorous based species resulting from NiPCy3 partial decomposition during milling have a major kinetic impact on MgH_2 dehydrogenation.
- The complex allows to disperse nickel at the surface of MgH_2 for a second kinetic impact, leading to further decrease of MgH_2 decomposition temperature.
- Finally, the presence of chlorine in NiPCy3 results on a negative impact on the decomposition kinetics of MgH_2.

Even if highly enhanced hydrogen storage properties are obtained by doping MgH_2 with only 5 wt% of NiPCy3 complex (absorption of 6.1 wt% of hydrogen within 5 min at 200 °C after cycling, desorption starting at 220 °C), the experiments showed that the improved dehydrogenation kinetics are not preserved during cycling. It is the result of the decomposition of the phosphorus based species, mostly catalyzing the decomposition kinetics of MgH_2.

The composite obtained by milling MgH_2 with Ni (10 wt%) and Fe (5 wt%) nanoparticles together with the NiPCy3 complex presented remarkable enhanced storage properties. 4 wt% of hydrogen is stored in less than 5 min at 100 °C while the hydrogen starts to be released below 200 °C. Minor changes in the hydrogen desorption behavior are observed during the first 3 sorption cycles before attaining complete reversibility. After 4 hydrogenation/dehydrogenation cycles, this storage system still presents the best performances among all the studied composites, with a maximum rate of hydrogen release at about 265 °C.

The results obtained in this study show that mixing thermally stable transition metal complexes and metal hydrides such as MgH_2 offers promising perspectives for obtaining a highly stable and performant storage system.

Conflicts of interest

There are no conflicts to declare.

Acknowledgements

This work was supported by the French Agence Nationale de la Recherche [Projet ANR-15-CE29-0023-01]. The authors are thankful for the scientific services of IRCELYON, particularly Y. Aizac for the XRD analyses, L. Burel for the SEM and TEM analyses and C. Lorentz for the NMR analyses. Dr C. Dupuis from McPhy Company is acknowledged for fruitful discussions.

References

[1] Dutta S. A review on production, storage of hydrogen and its utilization as an energy resource. J Ind Eng Chem 2014;20:1148–56. doi:10.1016/j.jiec.2013.07.037.

[2] Bakenne A, Nuttall W, Kazantzis N. Sankey-Diagram-based insights into the hydrogen economy of today. Int J Hydrogen Energy 2016;41:7744–53. doi:10.1016/j.ijhydene.2015.12.216.

[3] Acar C, Dincer I. Review and Evaluation of Hydrogen Production Options for Better Environment. J Clean Prod 2019. doi:10.1016/j.jclepro.2019.02.046.

[4] Parra D, Valverde L, Pino FJ, Patel MK. A review on the role, cost and value of hydrogen energy systems for deep decarbonisation. Renew Sustain Energy Rev 2019;101:279–94. doi:10.1016/j.rser.2018.11.010.

[5] Voloshin RA, Rodionova MV, Zharmukhamedov SK, Nejat Veziroglu T, Allakhverdiev SI. Review: Biofuel production from plant and algal biomass. Int J Hydrogen Energy 2016;41:17257–73. doi:10.1016/j.ijhydene.2016.07.084.

[6] Zhang F, Zhao P, Niu M, Maddy J. The survey of key technologies in hydrogen energy storage. Int J Hydrogen Energy 2016;41:14535–52. doi:10.1016/j.ijhydene.2016.05.293.

[7] Ren J, Musyoka NM, Langmi HW, Mathe M, Liao S. Current research trends and perspectives on materials-based hydrogen storage solutions: A critical review. Int J Hydrogen Energy 2017;42:289–311. doi:10.1016/j.ijhydene.2016.11.195.

[8] Dadashzadeh M, Kashkarov S, Makarov D, Molkov V. Risk assessment methodology for onboard hydrogen storage. Int J Hydrogen Energy 2018;43:6462–75. doi:10.1016/j.ijhydene.2018.01.195.

[9] Gurz M, Baltacioglu E, Hames Y, Kaya K. The meeting of hydrogen and automotive: A review. Int J Hydrogen Energy 2017;42:23334–46. doi:10.1016/j.ijhydene.2017.02.124.

[10] Yartys VA, Lototskyy MV, Akiba E, Albert R, Antonov VE, Ares JR, et al. Magnesium based materials for hydrogen based energy storage: Past, present and future. Int J Hydrogen Energy 2019. doi:10.1016/j.ijhydene.2018.12.212.

[11] Jain IP, Lal C, Jain A. Hydrogen storage in Mg: A most promising material. Int J Hydrogen Energy 2010;35:5133–44. doi:10.1016/j.ijhydene.2009.08.088.

[12] Crivello J-C, Denys RV, Dornheim M, Felderhoff M, Grant DM, Huot J, et al. Mg-based compounds for hydrogen and energy storage. Appl Phys A 2016;122:85(1-17). doi:10.1007/s00339-016-9601-1.

[13] Crivello J-C, Dam B, Denys RV, Dornheim M, Grant DM, Huot J, et al. Review of magnesium hydride-based materials: development and optimisation. Appl Phys A 2016;122:97(1-20). doi:10.1007/s00339-016-9602-0.

[14] Zhang J, Yan S, Qu H. Stress/strain effects on thermodynamic properties of magnesium hydride: A brief review. Int J Hydrogen Energy 2017;42:16603–10. doi:10.1016/j.ijhydene.2017.05.174.

[15] Zhang J, Yan S, Qu H. Recent progress in magnesium hydride modified through catalysis and nanoconfinement. Int J Hydrogen Energy 2018;43:1545–65. doi:10.1016/j.ijhydene.2017.11.135.

[16] Zhang J, Zhu Y, Yao L, Xu C, Liu Y, Li L. State of the art multi-strategy improvement of Mg-based hydrides for hydrogen storage. J Alloys Compd 2019;782:796–823. doi:10.1016/j.jallcom.2018.12.217.

[17] Thongtan P, Dansirima P, Thiangviriya S, Thaweelap N, Suthummapiwat A, Plerdsranoy P, et al. Reversible hydrogen sorption and kinetics of hydrogen storage tank based on MgH_2 modified by TiF_4 and activated carbon. Int J Hydrogen Energy 2018;43:12260–70. doi:10.1016/j.ijhydene.2018.04.171.

[18] Lutz M, Bhouri M, Linder M, Bürger I. Adiabatic magnesium hydride system for hydrogen storage based on thermochemical heat storage: Numerical analysis of the dehydrogenation. Appl Energy 2019;236:1034–48. doi:10.1016/j.apenergy.2018.12.038.

[19] Liu Y, Cao Y, Huang L, Gao M, Pan H. Rare earth–Mg–Ni-based hydrogen storage alloys as negative electrode materials for Ni/MH batteries. J Alloys Compd 2011;509:675–86. doi:10.1016/j.jallcom.2010.08.157.

[20] Xu Y, Mulder FM. TiF_3 catalyzed MgH_2 as a Li/Na ion battery anode. Int J Hydrogen Energy 2018;43:20033–40. doi:10.1016/j.ijhydene.2018.09.003.
[21] Bogdanović B, Bohmhammel K, Christ B, Reiser A, Schlichte K, Vehlen R, et al. Thermodynamic investigation of the magnesium–hydrogen system. J Alloys Compd 1999;282:84–92. doi:10.1016/S0925-8388(98)00829-9.
[22] Afzal M, Mane R, Sharma P. Heat transfer techniques in metal hydride hydrogen storage: A review. Int J Hydrogen Energy 2017;42:30661–82. doi:10.1016/j.ijhydene.2017.10.166.
[23] Bérubé V, Radtke G, Dresselhaus M, Chen G. Size effects on the hydrogen storage properties of nanostructured metal hydrides: A review. Int J Energy Res 2007;31:637–63. doi:10.1002/er.1284.
[24] Callini E, Aguey-Zinsou K-F, Ahuja R, Ares JR, Bals S, Biliškov N, et al. Nanostructured materials for solid-state hydrogen storage: A review of the achievement of COST Action MP1103. Int J Hydrogen Energy 2016;41:14404–28. doi:10.1016/j.ijhydene.2016.04.025.
[25] Zhang Q, Xu Y, Wang Y, Zhang H, Wang Y, Jiao L, et al. Enhanced hydrogen storage performance of MgH_2Ni_2P/graphene nanosheets. Int J Hydrogen Energy 2016;41:17000–7. doi:10.1016/j.ijhydene.2016.07.133.
[26] Sadhasivam T, Kim H-T, Jung S, Roh S-H, Park J-H, Jung H-Y. Dimensional effects of nanostructured Mg/MgH_2 for hydrogen storage applications: A review. Renew Sustain Energy Rev 2017;72:523–34. doi:10.1016/j.rser.2017.01.107.
[27] Hanada N, Ichikawa T, Fujii H. Catalytic Effect of Nanoparticle 3d-Transition Metals on Hydrogen Storage Properties in Magnesium Hydride MgH_2 Prepared by Mechanical Milling. J Phys Chem B 2005;109:7188–94. doi:10.1021/jp044576c.
[28] Kumar S, Singh A, Tiwari GP, Kojima Y, Kain V. Thermodynamics and kinetics of nano-engineered $Mg-MgH_2$ system for reversible hydrogen storage application. Thermochim Acta 2017;652:103–8. doi:10.1016/j.tca.2017.03.021.
[29] Zhang X, Shen Z, Jian N, Hu J, Du F, Yao J, et al. A novel complex oxide $TiVO_{3.5}$ as a highly active catalytic precursor for improving the hydrogen storage properties of MgH_2. Int J Hydrogen Energy 2018;43:23327–35. doi:10.1016/j.ijhydene.2018.10.216.
[30] Chen M, Xiao X, Zhang M, Liu M, Huang X, Zheng J, et al. Excellent synergistic catalytic mechanism of in-situ formed nanosized Mg_2Ni and multiple valence titanium for improved hydrogen desorption properties of magnesium hydride. Int J Hydrogen Energy 2019;44:1750–9. doi:10.1016/j.ijhydene.2018.11.118.
[31] Ismail M, Mustafa NS, Juahir N, Yap FAH. Catalytic effect of $CeCl_3$ on the hydrogen storage properties of MgH_2. Mater Chem Phys 2016;170:77–82. doi:10.1016/j.matchemphys.2015.12.021.
[32] Wang J, Du Y, Sun L, Li X. Effects of F and Cl on the stability of MgH_2. Int J Hydrogen Energy 2014;39:877–83. doi:10.1016/j.ijhydene.2013.10.135.
[33] Sazelee NA, Idris NH, Md Din MF, Mustafa NS, Ali NA, Yahya MS, et al. Synthesis of $BaFe_{12}O_{19}$ by solid state method and its effect on hydrogen storage properties of MgH_2. Int J Hydrogen Energy 2018;43:20853–60. doi:10.1016/j.ijhydene.2018.09.125.
[34] Li L, Zhang Z, Jiao L, Yuan H, Wang Y. In situ preparation of nanocrystalline Ni@C and its effect on hydrogen storage properties of MgH_2. Int J Hydrogen Energy 2016;41:18121–9. doi:10.1016/j.ijhydene.2016.07.170.
[35] Zhang Q, Wang Y, Zang L, Chang X, Jiao L, Yuan H, et al. Core-shell Ni_3N@Nitrogen-doped carbon: Synthesis and application in MgH_2. J Alloys Compd 2017;703:381–8. doi:10.1016/j.jallcom.2017.01.224.
[36] Zhang Q, Zang L, Huang Y, Gao P, Jiao L, Yuan H, et al. Improved hydrogen storage properties of MgH_2 with Ni-based compounds. Int J Hydrogen Energy 2017;42:24247–55. doi:10.1016/j.ijhydene.2017.07.220.
[37] Xie L, Liu Y, Zhang X, Qu J, Wang Y, Li X. Catalytic effect of Ni nanoparticles on the desorption kinetics of MgH_2 nanoparticles. J Alloys Compd 2009;482:388–92. doi:10.1016/j.jallcom.2009.04.028.

[38] Zhang T, Isobe S, Jain A, Wang Y, Yamaguchi S, Miyaoka H, et al. Enhancement of hydrogen desorption kinetics in magnesium hydride by doping with lithium metatitanate. J Alloys Compd 2017;711:400–5. doi:10.1016/j.jallcom.2017.03.361.
[39] Wang Y, Wang Y, Wang X, Zhang H, Jiao L, Yuan H. Destabilization effects of $Mg(AlH_4)_2$ on MgH_2: Improved desorption performances and its reaction mechanism. Int J Hydrogen Energy 2014;39:17747–53. doi:10.1016/j.ijhydene.2014.08.117.
[40] Zhang B, Li W, Lv Y, Yan Y, Wu Y. Hydrogen storage properties of the mixtures MgH_2–Li_3N with different molar ratios. J Alloys Compd 2015;645, Supplement 1:S464–7. doi:10.1016/j.jallcom.2014.12.081.
[41] Puszkiel JA, Arneodo Larochette P, Gennari FC. Hydrogen storage properties of MgxFe (x: 2, 3 and 15) compounds produced by reactive ball milling. J Power Sources 2009;186:185–93. doi:10.1016/j.jpowsour.2008.09.101.
[42] Atias-Adrian IC, Deorsola FA, Ortigoza-Villalba GA, DeBenedetti B, Baricco M. Development of nanostructured Mg_2Ni alloys for hydrogen storage applications. Int J Hydrogen Energy 2011;36:7897–901. doi:10.1016/j.ijhydene.2011.01.047.
[43] Chen X, Zou J, Zeng X, Ding W. Hydrogen storage properties of a Mg-La-Fe-H nano-composite prepared through reactive ball milling. J Alloys Compd 2017;701:208–14. doi:10.1016/j.jallcom.2017.01.056.
[44] Kumar S, Jain A, Miyaoka H, Ichikawa T, Kojima Y. Catalytic effect of bis (cyclopentadienyl) nickel II on the improvement of the hydrogenation-dehydrogenation of Mg-MgH_2 system. Int J Hydrogen Energy 2017;42:17178–83. doi:10.1016/j.ijhydene.2017.05.090.
[45] Galey B, Auroux A, Sabo-Etienne S, Grellier M, Dhaher S, Postole G. Impact of the addition of poly-dihydrogen ruthenium precursor complexes on the hydrogen storage properties of the Mg/MgH_2 system. Sustain Energy Fuels 2018;2:2335–44. doi:10.1039/C8SE00170G.
[46] Azadi G, Bagheri R, Bikas R, Mousazade Y, Cui J, Song Z, et al. A transparent electrode with water-oxidizing activity. Int J Hydrogen Energy 2018;43:22896–904. doi:10.1016/j.ijhydene.2018.10.146.
[47] Najafpour MM, Renger G, Hołyńska M, Moghaddam AN, Aro E-M, Carpentier R, et al. Manganese Compounds as Water-Oxidizing Catalysts: From the Natural Water-Oxidizing Complex to Nanosized Manganese Oxide Structures. Chem Rev 2016;116:2886–936. doi:10.1021/acs.chemrev.5b00340.
[48] Quasdorf KW, Tian X, Garg NK. Cross-Coupling Reactions of Aryl Pivalates with Boronic Acids. J Am Chem Soc 2008;130:14422–3. doi:10.1021/ja806244b.
[49] Xiao J, Wu J, Zhao W, Cao S. $NiCl_2(PCy_3)_2$-catalyzed hydrodefluorination of fluoroarenes with LiAl(O-t-Bu)3H. J Fluor Chem 2013;146:76–9. doi:10.1016/j.jfluchem.2012.12.002.
[50] Kissinger HE. Reaction Kinetics in Differential Thermal Analysis. Anal Chem 1957;29:1702–6. doi:10.1021/ac60131a045.
[51] Farjas J, Roura P. Exact analytical solution for the Kissinger equation: Determination of the peak temperature and general properties of thermally activated transformations. Thermochim Acta 2014;598:51–8. doi:10.1016/j.tca.2014.10.024.
[52] Chen B-H, Chuang Y-S, Chen C-K. Improving the hydrogenation properties of MgH_2 at room temperature by doping with nano-size ZrO_2 catalyst. J Alloys Compd 2016;655:21–7. doi:10.1016/j.jallcom.2015.09.163.
[53] He D, Wang Y, Wu C, Li Q, Ding W, Sun C. Enhanced hydrogen desorption properties of magnesium hydride by coupling non-metal doping and nano-confinement. Appl Phys Lett 2015;107:243907(1-5). doi:10.1063/1.4938245.
[54] Ma L-P, Kang X-D, Dai H-B, Liang Y, Fang Z-Z, Wang P-J, et al. Superior catalytic effect of TiF_3 over $TiCl_3$ in improving the hydrogen sorption kinetics of MgH_2: Catalytic role of fluorine anion. Acta Mater 2009;57:2250–8. doi:10.1016/j.actamat.2009.01.025.
[55] Xie L, Li J, Zhang T, Kou H. Role of milling time and Ni content on dehydrogenation behavior of MgH_2/Ni composite. Trans Nonferrous Met Soc China 2017;27:569–77. doi:10.1016/S1003-6326(17)60063-3.

Graphical abstract